# SHAKING TABLE TEST OF SMALL SCALED HPFRCC COLUMN

Noriko TOKUI[1], Yoshiaki NAKANO[2], Yasushi SANADA[3], Yuki SAKAI[4], Haruhiko SUWADA[5] and Hiroshi FUKUYAMA[6]

**ABSTRACT**: To establish a simple and cost effective testing technique to investigate seismic behaviors of RC structures, extremely small scaled model structures consisting of high performance fiber reinforced cement composite (HPFRCC) material reinforced only with longitudinal reinforcement are fabricated, and their dynamic behaviors are experimentally and analytically investigated.

**Key Words**: Reinforced concrete, Shaking table test, Scaled model, HPFRCC

## INTRODUCTION

Shaking table tests have been widely applied to investigate dynamic behaviors of structures under earthquake excitations. In the shaking table tests of reinforced concrete (R/C) structures, relatively large specimens are generally tested to eliminate difficulties in fabricating specimens. However, the number of shaking tables that have enough capacity to carry out large-scale tests are limited, and much cost and time are generally required. Even when shaking table tests using relatively small specimen are carried out, it may be difficult to provide lateral reinforcement in such a scaled specimen. Therefore another methodology is needed to carry out shaking table tests within limited cost.

Recent investigations on high performance fiber reinforced cement composite (HPFRCC) material indicates that tension stiffening as well as multiple cracking effects of HPFRCC may result in ductile behavior. To establish a simple and cost effective testing technique to investigate seismic behaviors of RC structures, extremely small scaled model structures consisting of high performance fiber reinforced cement composite (HPFRCC) material reinforced only with longitudinal reinforcement are fabricated, and their dynamic behaviors are experimentally and analytically investigated.

## TEST SPECIMENS

In this study, two types of specimens are designed as shown in Figure 1: Type-S (stub) specimen has stubs at both top and bottom ends, and Type-P (plate) specimen has plates at both top and bottom ends. Each specimen has a cross section of 30 x 30 mm and the height $h$ of 180 mm. The shear-span-to-depth ratio of each specimen is 3.0, and the tensile reinforcement ratio is 2.19%.

Extremely small-scaled column specimens investigated in this study are not the simply size-reduced

[1] Graduate Student, Graduate School of Engineering, University of Tokyo,
[2] Associate Professor, Institute of Industrial Science, University of Tokyo, Dr. Eng.
[3] Research Associate, Earthquake Research Institute, University of Tokyo, Dr. Eng.
[4] Associate Professor, Institute of Engineering Mechanics and Systems, University of Tsukuba, Dr. Eng.
[5] Researcher, National Institute for Land and Infrastructure Management, Ministry of Land, Infrastructure and Transport
[6] Chief Researcher, Building Research Institute, Dr. Eng.

models of existing full-scale R/C members but those consisting of longitudinal steel reinforcement and HPFRCC material without lateral reinforcement. As they do not have tranverse reinforcement, very small specimens can be made with less work and lower costs. Therefore, this method may enable to conduct shaking table tests of simple structures under various sets of input ground motions or those of multi-storied and spanned buildings, which have been generally difficult to perform with ordinary scaled specimens.

In this study, three Type-S specimens and six Type-P specimens are made, and their behaviors are investigated under shaking table tests and static loading tests.

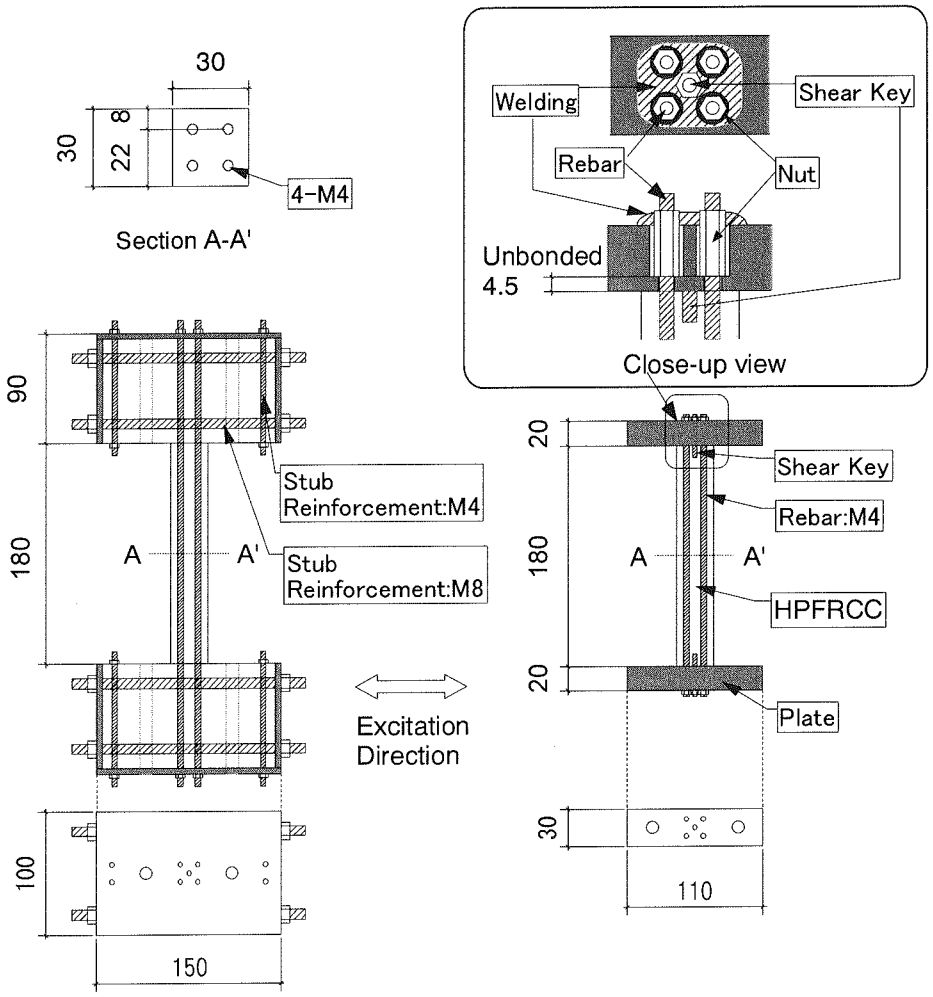


**Figure 1.** Dimension of specimens

*Material*

Tables 1 and 2 summarize the material properties of HPFRCC and longitudinal reinforcement bars obtained in the static material test, where the average values of three samples are shown.

The HPFRCC is mortar matrix (water-cement ratio: 45%, and sand-cement ratio: 40%) mixed with 1.0% volume ratio of polyethylene fiber (fiber length: 15mm, and diameter of a fiber: 12 $\mu$m). The cylinder size of material tests is 100mm x 200mm (diameter x height).

The longitudinal reinforcement used in specimens is metric coarse screw threads with major diameter (d) of external thread of 4mm. The detail information of screw threads can be found in the Japanese Industrial Standards (JIS) B 0205 as shown in Figure 2.

The metric coarse screw threads with a diameter of 4mm and 8mm are used for the stub reinforcement in Type-S specimen. The thickness of the steel plate in Type-P specimen is 20mm.

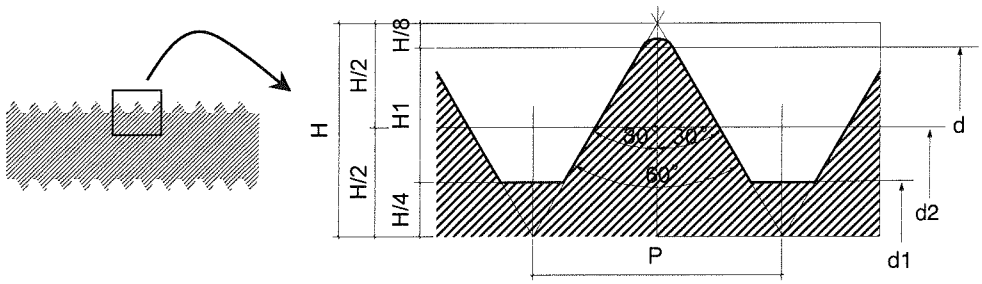


| | Pitch<br>P | Thread Overlap<br>H1 | Major Diameter of External Thread<br>d | Pitch Diameter<br>d2 | Major Diameter of Internal Thread<br>d1 |
|---|---|---|---|---|---|
| M4 | 0.7 | 0.379 | 4.0 | 3.545 | 3.242 |
| M8 | 1.25 | 0.677 | 8.0 | 7.188 | 6.647 |

**Figure 2.** The detail information of screw threads[4)]

**Table 1.** Material properties of HPFRCC

| Loading Pattern | Specimen | Age (days) | Young's Modulus *1 $E_c$ (N/mm$^2$) | Compressive Strength $\sigma_B$ (N/mm$^2$) | Strain at Compressive Strength $\varepsilon_B$ (%) | Tensile Strength $\sigma_t$ (N/mm$^2$) | Strain at Ultimate Tensile Strength $\varepsilon_{ut}$ (%) |
|---|---|---|---|---|---|---|---|
| Dynamic | Type-S | 19 | $1.95\times10^4$ | 45.74 | 0.34 | 2.00 | $\geqq 2.0$[2)] |
| | Type-P | 18 | $1.69\times10^4$ | 47.68 | 0.40 | 2.14 | |
| Static | Type-S | 16 | $1.75\times10^4$ | 48.74 | 0.42 | - *2 | |
| | Type-P | 18 | $1.69\times10^4$ | 47.68 | 0.40 | 2.14 | |

*1 secant modulus at 1/3 $\sigma_B$

*2 not measured

**Table 2.** Material Properties of Longitudinal reinforcement

| | Cross Section Area (mm$^2$) | Young's Modulus $E_s$ (N/mm$^2$) | Yield Strength *1 $\sigma_y$ (N/mm$^2$) | Yield Strain $\varepsilon_y$ (%) |
|---|---|---|---|---|
| M4 | 9.87 | $1.35\times10^5$ | 443.8 | 0.55 |

*1 0.2% off-set value

*Fabrication Process of Specimens*

The specimen and its forms are designed by assembling steel plate and aluminum channel bars and angles. Figures 3 and 4 show the form for Type-P specimen and Type-S specimen, respectively. Followings are the fabrication steps for Type-P specimen (Figure5).

1. Bolt aluminum channel bars on a base plate.
2. Coat the inner surfaces of the form with grease.
3. Place the steel plates at both ends of the channel bars.
4. Set four longitudinal reinforcing bars through the hole of end plate and fix them tightly with nuts.
5. Set shear-keys with epoxy adhesive.
6. Mix the HPFRCC.
7. Cast the HPFRCC and cure carefully by wet cloth. After a week, remove the casting form.
8. Finally, weld the nuts with end plates of Type-P specimen. Stubs are provided at both ends of Type-S specimen, as is done in general specimen (Figure4).

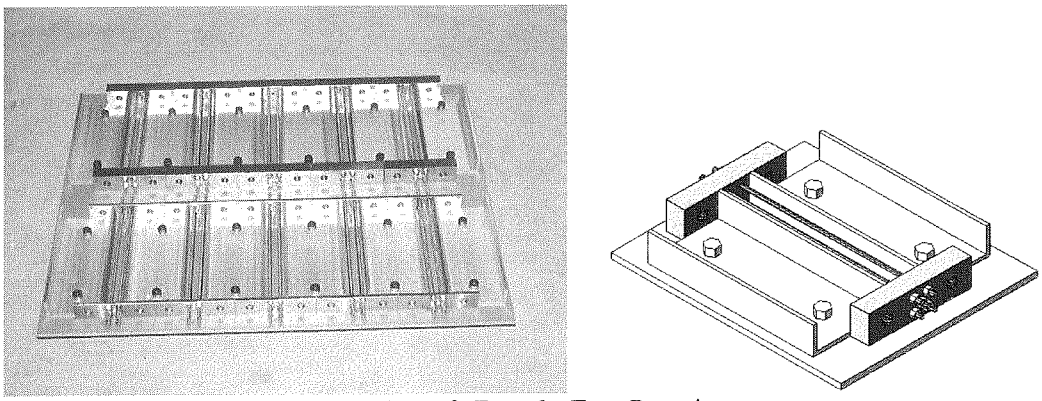

**Figure 3.** Form for Type-P specimen

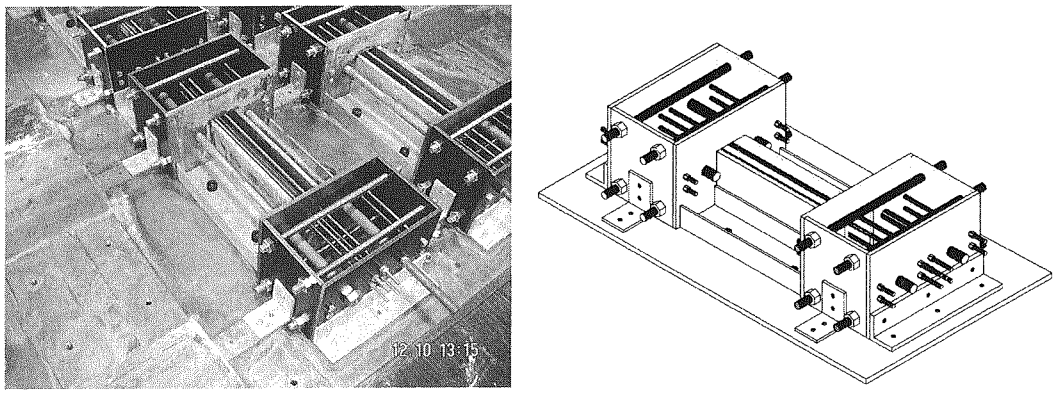

**Figure 4.** Form for Type-S specimen

1.Assemblage of channel bars

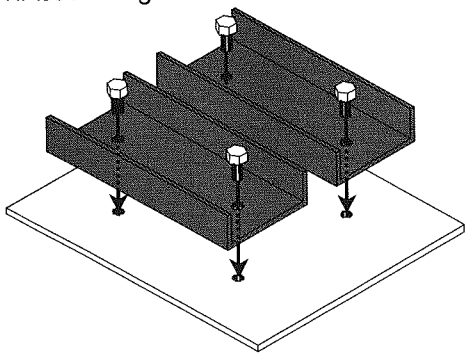

2.Coating with grease

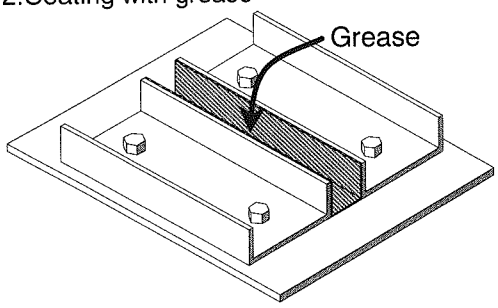


3.Assemblage of end plates

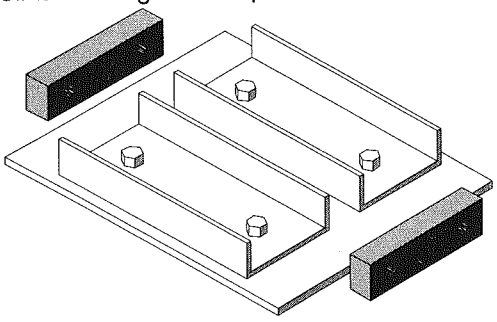

4.Arrangement of Reinforcement

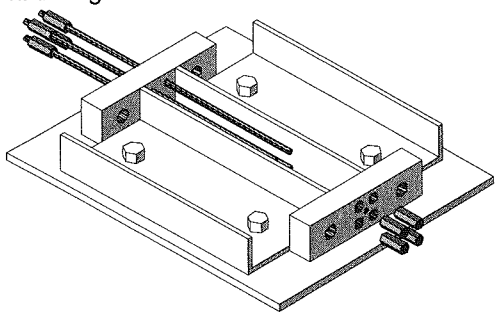

5.Attachment of shear keys

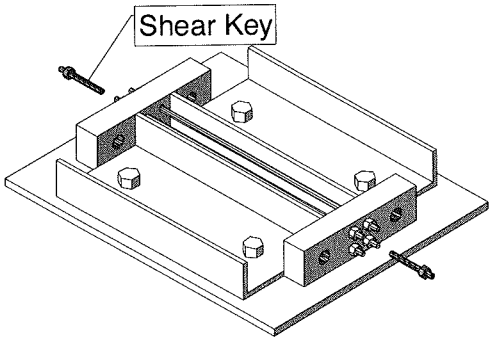


6.Mixing of HPFRCC

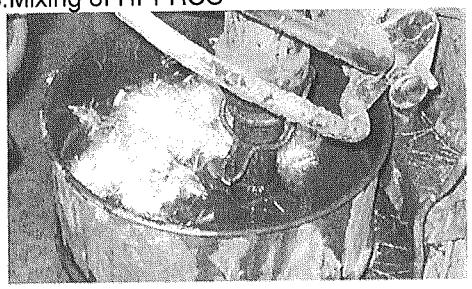

7.Casting of HPFRCC

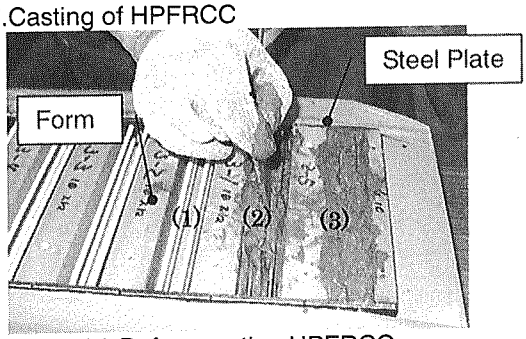


(1) Before casting HPFRCC
(2) Under casting HPFRCC
(3) After casting HPFRCC

8.Welding of nuts with end plates

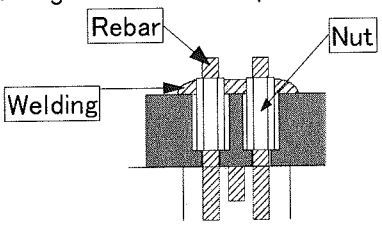


**Figure 5.** Fabrication of Type-P specimen

## SHAKING TABLE TEST

### Test Setup

Test setup is shown in Figure 6. Each specimen is placed on and fixed to component (c). This system has horizontal and vertical sliders, which enable specimens to deform in the lateral and axial direction when they are subjected to anti-symmetric bending during excitations.

For shaking table tests, it is important to measure an inertia force of specimen. Because of the complexity of test setup, it is necessary to confirm that the friction of sliders is negligible and does not affect the excitation system. A new system using load cells is therefore developed to directly record the inertia force acting on the specimen. Load cells (1) and (2) are installed at both ends of the component (c), which is placed on horizontal sliders, and the compression force of 2940N is introduced between them. The inertia force can be obtained considering the difference between two measured forces, as will be described later.

The relative displacement $y$ of specimen is measured horizontally between point (a) and component (c). Accelerometers are installed at point (a), (d), and the shaking table. To observe the effects of different design details at specimen ends, i.e., stub end and plate end, the rotation angle $\theta_{h'}$ at 10mm above the column base is measured as shown in Figure 7. These data are recorded with a sampling interval of 0.002 seconds.

### *Test Program*

In this experiment, the overall weight $W$ of a specimen including self-weight and equipment weight is 3234N. The calculated initial period of the specimen is 0.074 seconds. The sinusoidal wave of which amplitude increases gradually as shown in Figure 8 is used to excite specimens. The period of the sinusoidal wave is 0.2 seconds, which is about 3 times of the calculated period of specimens.

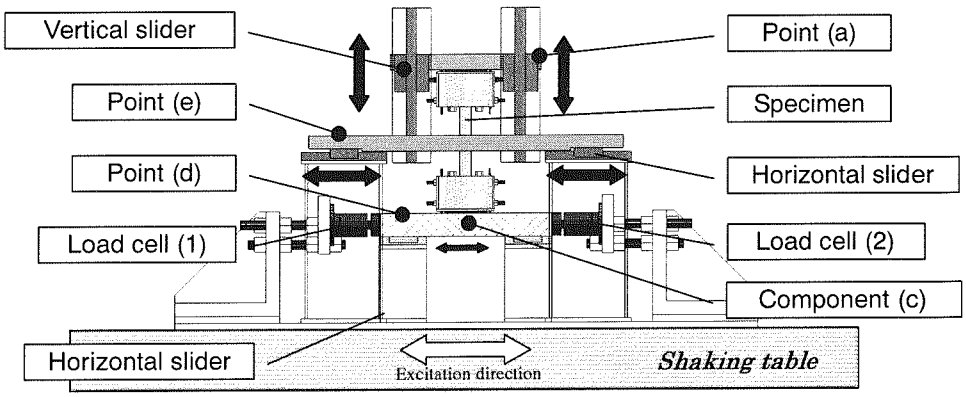


**Figure 6.** Test setup

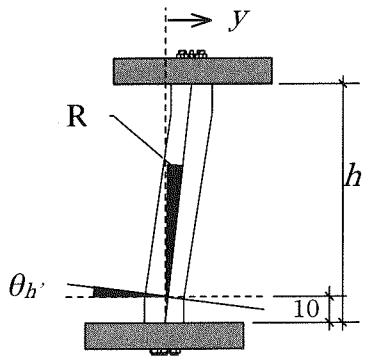


**Figure 7.** Rotation angle measurement

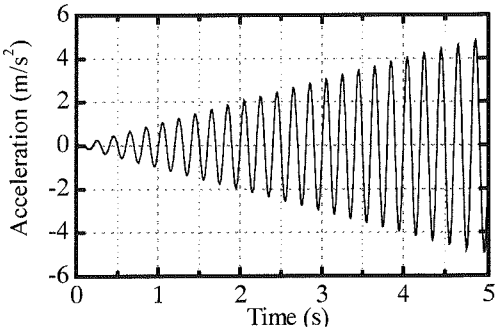


**Figure 8.** Input sinusoidal wave

***Test Results***

In the experiment, inertia forces (i.e., restoring and damping forces) of specimens are evaluated in two methods, and then results are compared to confirm that the friction of sliders are negligible.

**Method I:** The inertia force $Q_1$ is simply obtained by the product of the overall mass of specimen $M$ ($M$=overall weight $W$ / gravity $G$) and the absolute acceleration $a$ recorded at point (a).

$$Q_1 = Ma \tag{1}$$

**Method II:** The inertia force $Q_2$ is calculated based on the forces of load cells, the inertia force acting on lower stub and component (c), and the damping force from sliders as shown in Eq. (2). Forces acting on the system are illustrated in Figure 9.

$$Q_2 - P_C + (P_{L1} - P_{L2} - P_{DS}) = 0 \tag{2}$$

$$P_C = m_C \cdot a_C$$

where,

$P_C$: inertia force acting on lower stub and component (c), $P_{L1}$: force obtained from load cell (1), $P_{L2}$: force obtained from load cell (2), $P_{DS}$: damping force from slider, $m_C$: mass of stub and component (c), $a_C$: absolute acceleration of stub and component (c)

Assuming $P_{DS} \approx 0$, Eq. (2) can be rewritten as Eq. (3).

$$Q_2 \approx (-P_{L1} + P_{L2}) + P_C \tag{3}$$

To compare these inertia forces, the time history of shear coefficient $C$ (inertia force ($Q_1$ or $Q_2$) /W) is shown in Figure 10. This figure shows that the two inertia forces are approximately same and the friction of sliders is negligibly small as assumed in Eq. (3). It should be noted, however, that the waveform of $Q_2$ is smoother than that of $Q_1$ in large amplitude region, and $Q_2$ results is used hereafter to discuss the dynamic behaviors of specimen.

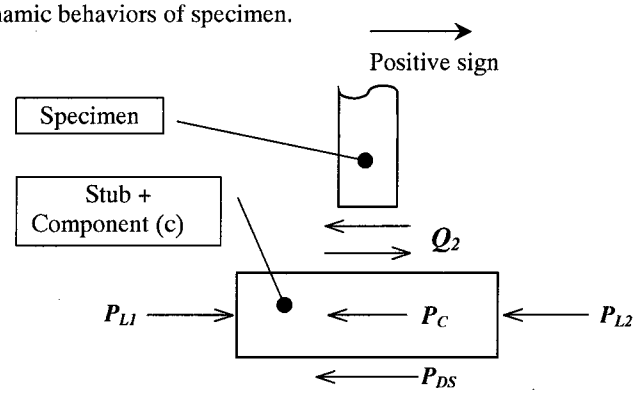


**Figure 9.** Forces acting on the system

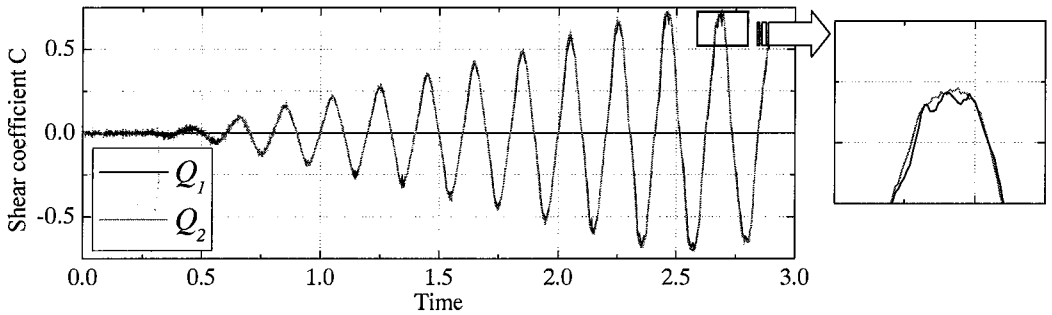


**Figure 10.** Comparison of $Q_1$ with $Q_2$

Figure 11 shows the relationship of response shear coefficient $C$ (= $Q_2$ / $W$) and drift angle $R$ (= $y$ / $h$) of each specimen. Both specimens show ductile behaviors with spindle shaped hysteretic loops. The maximum value $C_{MAX}$ of Type-S specimen (0.707) is 20% larger than that of Type-P specimen (0.656) although they have the same sectional and material properties. To understand the reason of different $C_{MAX}$ values, static loading tests of both specimens are carried out and their fundamental behaviors are carefully investigated later.

To compare the fundamental characteristics of extremely small-scaled specimens proposed herein to those of general R/C members, the following three parameters $\alpha_y$, $\beta$, and $h_{eq}$ are calculated and summarized in Table 3 and Figure 12. They are defined as:

(1) $\alpha_y$: the ratio of secant stiffness at yielding to the initial stiffness
(2) $\beta$: the ratio of post-peak stiffness to the initial stiffness
(3) $h_{eq}$: equivalent damping factor

The yielding of the specimen is defined as the point where its instant stiffness is lower than 10% of the initial stiffness. Table 3 reveals that the specimens successfully simulate the fundamental characteristics of R/C members since the parameters $\alpha_y$ and $\beta$ generally lie in the range of 0.2 to 0.4 and 0.00 to 0.05, respectively.

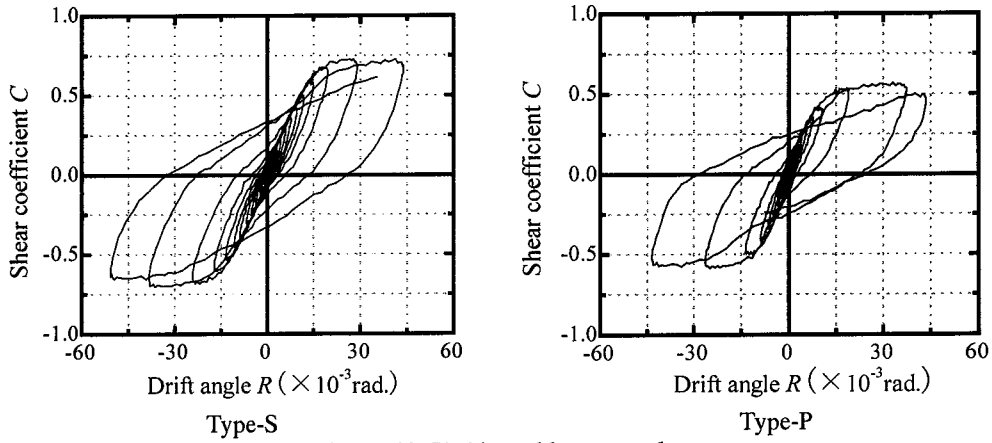


**Figure 11.** Shaking table test results

**Table 3.** Degradation in stiffness

| | $\alpha_y$ | $\beta$ |
|---|---|---|
| Type-S specimen | 0.25 | 0.040 |
| Type-P specimen | 0.23 | 0.033 |

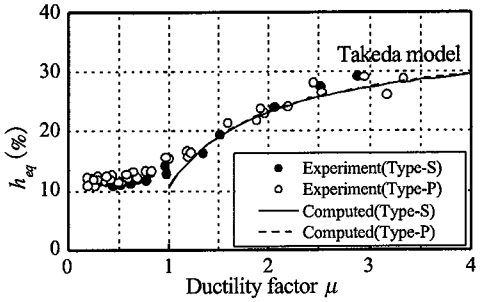


**Figure 12.** Equivalent damping factor

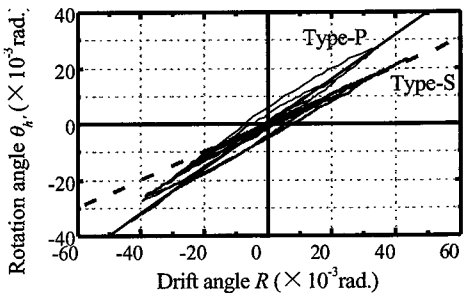


**Figure 13.** $\theta_{h'}$ - R relationship

Figure 12 shows the relationship of $h_{eq}$ between test results and computed values based on Takeda model, where the hysteretic loop is characterized by the stiffness degradation factor $\alpha$ of 0.0 under unloading and the damping factor $h$ of 0.05, which may correspond to a relatively fat shape, as well as $\alpha_y$ and $\beta$ described in Table 3. The test results show good agreement with the computed results. Note that other experiments preliminarily carried out by the authors show that the less fat hysteretic loop can be reproduced by reducing the mixture volume of fiver material.

Figure 13 shows the $\theta_h$ - $R$ relationship of both specimens. This figure shows that the ratio of $\theta_h$ of Type-P specimen to that of Type-S specimen lies in the range of 1.5 to 2.0, and the deformation is more significantly concentrated over the end regions for Type-P specimen.

## STATIC LOADING TEST

In the shaking table test, the $Q_{MAX}$ of Type-S specimen is 20% larger than that of Type-P specimen although they have the same sectional and material properties. To evaluate the difference in $Q_{MAX}$ values, static loading tests of both specimens are carried out.

### *Specimen and Test Setup*

The specimens used in static loading tests are the same as those of shaking table tests. For the static tests, the equipment shown in Figure 14 is attached at the point (e) indicated in Figure 6. The displacements obtained in the shaking table tests are applied to each specimen by pushing and pulling point (e). The displacements are imposed with a PC rod by tightening and loosening a nut placed at the reaction wall. After the maximum displacement experienced during the shaking table test is imposed, each specimen is monotonically loaded to collapse.

### *Test Result*

Table 4 shows the maximum $Q$ values ($Q_{MAX}$ ) of specimens during shaking table test and static loading test. Figure 15 shows the $C$ - $R$ relationship of each specimen.

As can be found in comparison between shaking table test and static loading test shown in Table 4, $Q_{MAX}$ during the shaking table test is 8% higher for Type-S specimen while it is almost the same for Type-P specimen. This result implies that the effect of strain rate may be different in Type-S and Type-P specimens.

Table 4 and Figure 15 show that the maximum value of $C$ of Type-S specimen during static loading test is 11% higher than that of Type-P specimen. The higher strength in Type-S specimen may be attributed to the different design details at specimen ends; the Type-S specimen has stub ends where fiber reinforced cement is monolithically cast together with its mid-column part, and the critical sections at both ends can therefore resist tensile actions to some extent even in the post-crack stage, while the Type-P specimen has steel plate ends which do not contribute to the resistance of cracked section.

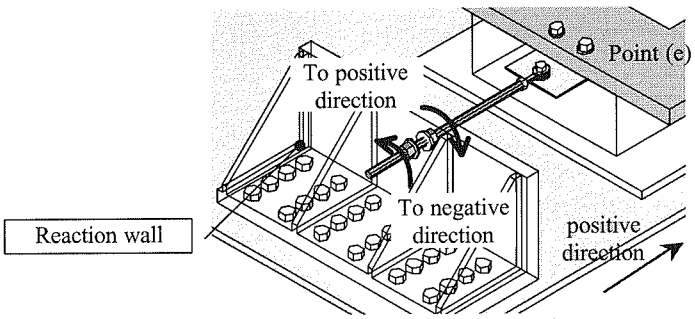


**Figure14.** Static loading equipment

**Table 4.** Comparison of maximum $Q$ values

| | $Q_{MAX}$ (N) [$C_{MAX}$] | | (Shaking Table Test) / (Static Test) |
|---|---|---|---|
| | Shaking Table Test | Static Test | |
| Type-S specimen | 2285 [0.707] | 2122 [0.656] | 1.08 |
| Type-P specimen | 1897 [0.587] | 1911 [0.591] | 0.99 |
| (Type-S) / (Type-P) | 1.20 | 1.11 | - |

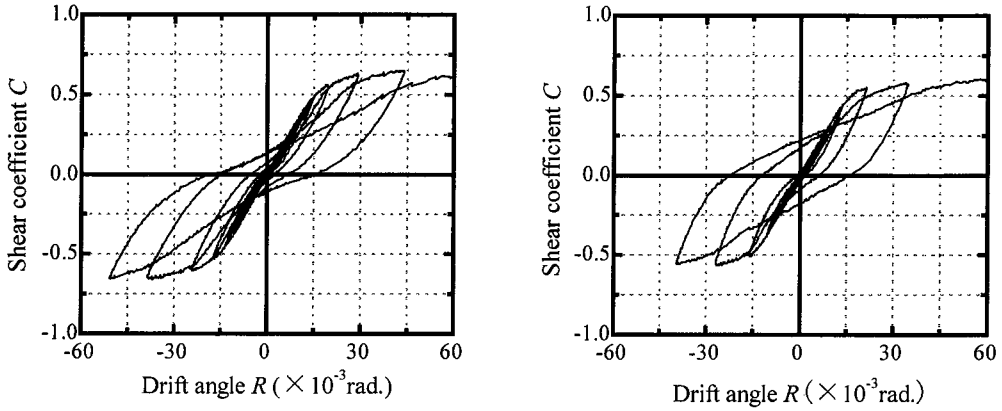


**Figure15.** Static loading test results

## FIBER MODEL ANALYSIS CONSIDERING STRAIN RATE EFFECTS

To investigate the difference in $Q_{MAX}$ due to design details at specimen ends and strain rate effects, fiber model analyses are carried out.

### *Assumptions in Computation*

### *Curvature Distributions*

Figure 16 shows the curvature distributions assumed in the analysis. As can be found in the figure, a triangular curvature distribution is assumed for Type-S specimens, while a combined profile of rectangular and triangular distribution is assumed for Type-P specimen since the longitudinal reinforcement is unbonded to HPFRCC over the unbonded length of $h_p$ (4.5mm) in the end plates as shown in Figure 1.

The curvature ${}_s\phi_0$ at the critical section of Type-S specimen at a given displacement ${}_sy$, and the rotation angle ${}_s\theta_{h'}$ at $h'$ (=10 mm) above the column base, is determined by Eqs. (3) and (4), respectively, assuming the curvature distribution shown in Figure 16(a).

$$ {}_s\phi_0 = \frac{3 \cdot {}_sy}{h^2} \tag{3} $$

$$ {}_s\theta_{h'} = \frac{1}{2} {}_s\phi_0 \cdot h' \left( 2 - \frac{h'}{h} \right) = \frac{3}{2} \frac{{}_sy}{h} \cdot \frac{h'}{h} \left( 2 - \frac{h'}{h} \right) \tag{4} $$

Based on the curvature distribution shown in Figure 16(b), the drift ${}_py$ and the rotation angle ${}_p\theta_{h'}$ at a distance of $h'$ (=10 mm) from the bottom stub of Type-P specimen are obtained as Eqs. (5) and (6).

$$ {}_{P}y = \frac{1}{3}{}_{p}\phi_0 h^2 + {}_{p}\phi_{hp} \cdot h_p \left( h + \frac{h_p}{2} \right) \tag{5} $$

$$ {}_{P}\theta_{h'} = \frac{1}{2}{}_{p}\phi_0 \cdot h' \left( 2 - \frac{h'}{h} \right) + {}_{p}\phi_{hp} \cdot h_p \tag{6} $$

where, ${}_{p}\phi_0$ and ${}_{p}\phi_{hp}$ are curvatures at critical section and at $h_p$ below the end plate, respectively. Considering the experimental results shown in Figure 13, the relation of ${}_{p}\theta_{h'}$ and ${}_{s}\theta_{h'}$ is assumed to be in the form of Eq. (7).

$$ {}_{P}\theta_{h'} = 2\,{}_{S}\theta_{h'} \tag{7} $$

Setting ${}_{p}y$ of Eq.(5) equal to ${}_{s}y$ of Eq.(3), the curvature ${}_{p}\phi_0$ at the critical section at a given displacement ${}_{p}y$ (=${}_{s}y$ ) is then obtained from Eqs. (4) to (7). The location of the neutral axis and the strain of each fiber segment are determined based on the curvature at the critical section ${}_{s}\phi_0$ (or ${}_{p}\phi_0$) obtained above, the equilibrium condition of axial force of a section, and the plane section assumption.

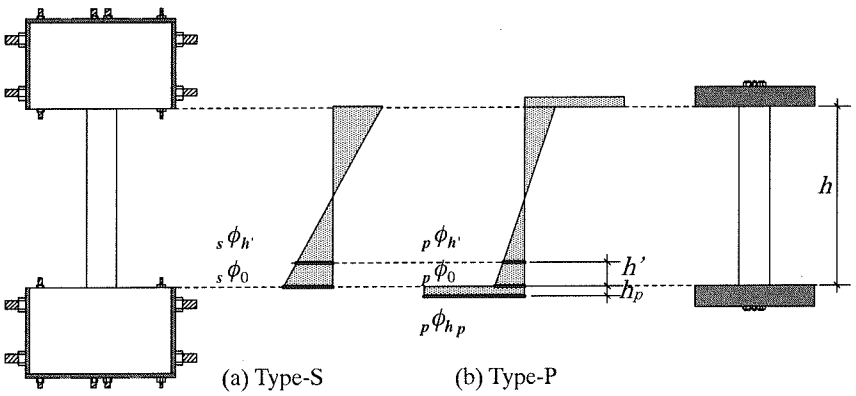


(a) Type-S (b) Type-P

**Figure 16.** Curvature distribution

***Material Characteristics***

Figure 17 shows the modeling at the critical section employed in these analyses. To consider strain rate effects on the material's $\sigma$ - $\varepsilon$ relationship, the strain rate ${}_{k}\dot{\varepsilon}$ is calculated by Eq. (8).

$$ {}_{k}\dot{\varepsilon} = \Delta_k \varepsilon / \Delta t \tag{8} $$

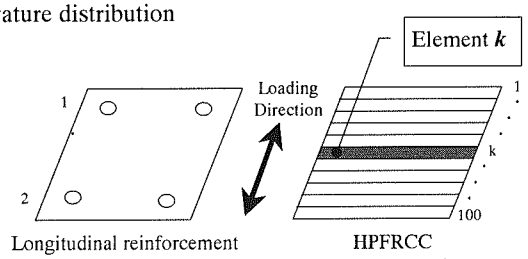


**Figure 17.** Modeling at the critical section

where, $\Delta_k \varepsilon$ and $\Delta t$ are the strain increment of element $k$ and the time increment, respectively.

Figure 18 shows material properties model for HPFRCC and longitudinal reinforcement. In compression, the $\sigma$ - $\varepsilon$ relation of HPFRCC is represented with (1) a linear line having a slope of initial Young's modulus $E_c$, (2) a parabola curve that passes through the origin (0, 0) and the peak ($\varepsilon_B$, $\sigma_B$), (3) a linearly falling branch, and (4) a residual strength plateau with $0.5\sigma_B$. In tension, a tensile strength of 0.05 $\sigma_B$ after yielding is assumed up to 2% for Type-S specimen, while the strength contribution is neglected for Type-P specimen. The Young's modulus $E_c$ and strength $\sigma_B$ shown in Table 1 is factored in accordance with strain rate, as shown in Eqs. (9) through (12).

In both tension and compression, the $\sigma$ - $\varepsilon$ relation of longitudinal reinforcement is represented with (1) a linear line having initial Young's modulus $Es$ and (2) a linear line with 0.01 $E_s$. The yield strength $\sigma_y$ show in Table 2 is factored in accordance with strain rate, as shown in Eq. (13).

***HPFRCC***

***Young's modulus***

$$|\dot{\varepsilon}| > 10^1 \mu/\sec \quad {}_d E_c = (0.02 \cdot \log|\dot{\varepsilon}| + 0.98) \cdot {}_s E_c$$
$$|\dot{\varepsilon}| \le 10^1 \mu/\sec \quad {}_d E_c = {}_s E_c \tag{9}$$

where, ${}_d E_c$ : Young's modulus of HPFRCC (dynamic)

${}_s E_c$ : Young's modulus of HPFRCC (static)

***compressive strength***

$$|\dot{\varepsilon}| > 10^1 \mu/\sec \quad {}_d\sigma_B = (0.06 \cdot \log|\dot{\varepsilon}| + 0.94) \cdot {}_s\sigma_B$$
$$|\dot{\varepsilon}| \le 10^1 \mu/\sec \quad {}_d\sigma_B = {}_s\sigma_B \tag{10}$$

where, ${}_d\sigma_B$ : Compressive strength of HPFRCC (dynamic)

${}_s\sigma_B$ : Compressive strength of HPFRCC (static)

***tensile strength***

· Type-S

$$\sigma_t = 0.05\sigma_B \quad (\sigma_B = {}_s\sigma_B \text{ or } {}_d\sigma_B) \tag{11}$$

· Type-P

$$\sigma_t = 0 \tag{12}$$

***Longitudinal Reinforcement***

***yield strength of longitudinal reinforcement***

$$|\dot{\varepsilon}| > 10^2 \mu/\sec \quad {}_d f_y = (0.05 \cdot \log|\dot{\varepsilon}| + 0.90) \cdot {}_s f_y$$
$$|\dot{\varepsilon}| \le 10^2 \mu/\sec \quad {}_d f_y = {}_s f_y \tag{13}$$

where, ${}_d f_y$ : Yield strength of longitudinal reinforcement (dynamic)

${}_s f_y$ : Yield strength of longitudinal reinforcement (static)

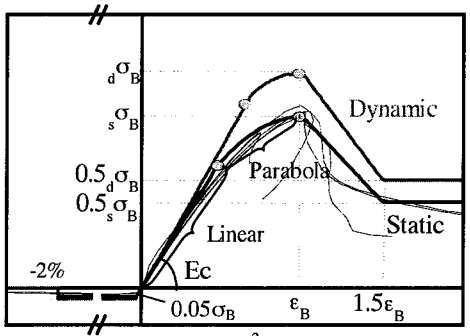


$${}_s\sigma_B = 47(N/mm^2),\ {}_s\varepsilon_B = 0.4(\%)$$

$$E_c = 1.8 \times 10^4 (N/mm^2)$$

HPFRCC

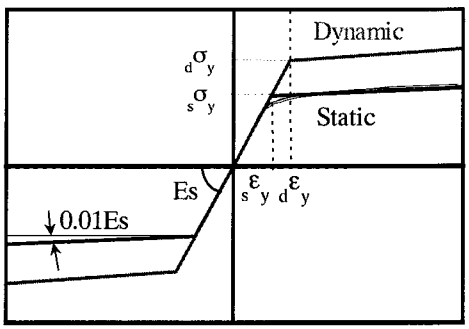


$${}_s\sigma_y = 450(N/mm^2)$$

$$E_s = 1.35 \times 10^5 (N/mm^2)$$

Longitudinal Reinforcement

**Figure 18.** Model of material properties

***Results and Discussions***

Computed results are compared with those of static loading tests and shaking table tests in Figures 19 and 20, respectively. Figure 21 shows the strain rate and its corresponding magnification factor of tensile reinforcement at the critical section of each specimen used in the computation.

As is found in Figure 19, $Q_{MAX}$ can be predicted considering the contribution of HPFRCC material to tension resistance in Type-S specimen and neglecting such contribution in Type-P specimen.

The computed $Q_{MAX}$ of Type-S specimen subjected to dynamic loading agrees well with the test result considering the strain rate effects. The strain rate and corresponding magnification factor of material strength is, as shown in Figure 21, generally lower in Type-P specimen, which is attributed to a curvature profile different from that assumed for Type-S specimen. Although the computed $Q_{MAX}$ of Type-P specimen is accordingly lower than that of Type-S specimen, it is still higher by 15% than experimental results. This result may be attributed to the overestimated strain rate effect in Type-P specimen, and the relation between the design detail at the unbonded region and strain rate effect needs to be further studied.

The computed stiffness of Type-P specimen subjected to both dynamic and static loading agrees well with the test result. However, the computed stiffness of Type-S specimen overestimates the test result. Therefore, curvature distributions assumed in the analysis need to be improved.

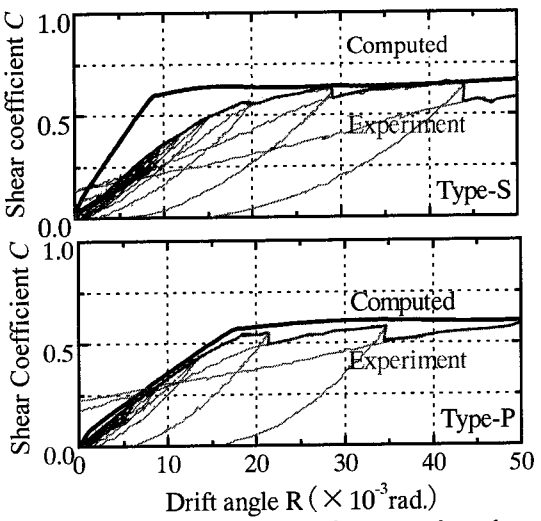


**Figure 19.** Comparison of computed results with static test result

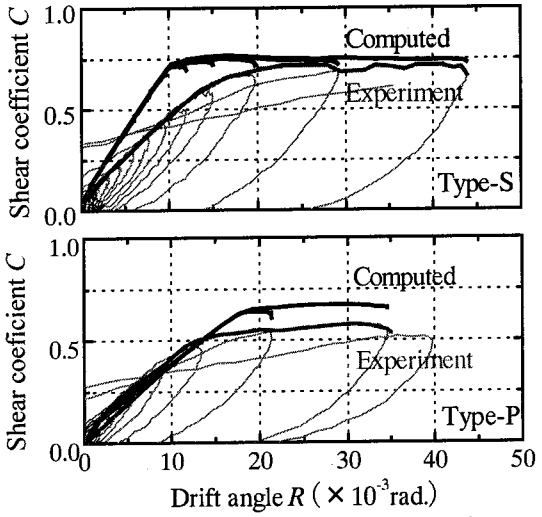


**Figure 20.** Comparison of computed results with shaking table test result

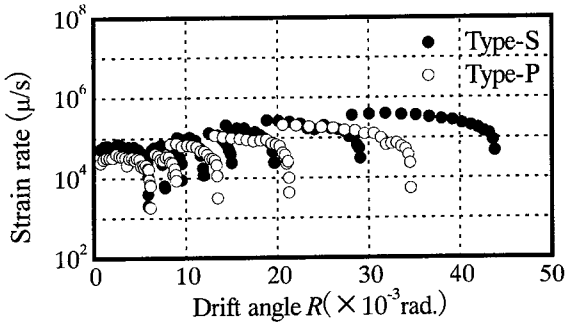


**Figure 21.** Computed strain rate of tensile reinforcement

## CONCLUSION

To establish a simple and cost effective testing technique to simulate seismic behaviors of R/C structures, extremely small-scaled model structures consisting of high performance fiber reinforced cement composite (HPFRCC) material reinforced only with longitudinal reinforcement are fabricated, and their behaviors are experimentally and analytically investigated.

1) The specimens in this study show ductile behaviors with spindle shaped hysteretic loops. The ratio of secant stiffness at yielding to the initial stiffness ($\alpha_y$) and that of post-peak stiffness to the initial stiffness ($\beta$) also successfully simulates those of typical R/C members. The equivalent damping factor ($h_{eq}$) of test results corresponds to the computed results that have a relatively fat hysteretic loop. Note that other experiments preliminarily carried out by the authors show that the less fat hysteretic loop can be reproduced by reducing the mixture volume of fiver material.
2) The rotational angle $\theta_{h'}$ of column is measured at a distance of 10 mm from its base, and compared in both specimens. The results show that the angle $\theta_{h'}$ of Type-P specimen is 1.5 to 2.0 times of that of Type-S specimen at the same drift angle. This is primarily due to the presence of longitudinal reinforcement unbonded to HPFRCC, and highly contributing to the concentrated deformation over the end region of Type-P specimen.
3) The maximum inertia force $Q_{MAX}$ of Type-S specimen observed during shaking table test is 20% larger than that of Type-P specimen although they have the same sectional and material properties. The computed $Q_{MAX}$ of Type-S specimen subjected to dynamic loading agrees well with the experimental result considering the strain rate effects. However, the computed $Q_{MAX}$ of Type-P specimen is about 15% higher than the experimental result. This result may be attributed to the overestimated strain rate effect in Type-P specimen, and the relation between the design detail at the unbonded region and strain rate effect needs to be further studied.
4) The maximum $Q$ values of Type-S specimen observed in static loading test is 11% larger than that of Type-P specimen. The computed $Q_{MAX}$ under static loading can be predicted considering the contribution of fiber reinforced cement composite material to tension resistance in Type-S specimen and neglecting such contribution in Type-P specimen.
5) The computed stiffness of Type-P specimen subjected to both dynamic and static loading agrees well with the test result. However, the computed stiffness of Type-S specimen overestimates the test result. Therefore, curvature distributions assumed in the analysis need to be improved

## ACKNOWLEDGEMENTS

The Central Workshop at the Institute of Industrial Science is also greatly appreciated for its technical support in fabricating specimens.

## REFERENCES

1. High Performance Fiber Reinforced Cement Composites (HPFRCC 2), A. E. Naaman and H. W. Reinhardt Ed., RILEM Proceeding 31, 1995
2. Sato, Y. Fukuyama, H. Suwada, H.: A Proposal of Tension-Compression Cyclic Loading Test Method for Ductile Cementitious Composite Materials, Journal of Structural and Construction Engineering, No.539, pp. 7-12, Jan., 2001
3. Hiroshi, H. Tuneo, O. Yoshikazu, K. Yoshiaki, N. Fumitoshi, K.: Fiber Model Analysis of Reinforced Concrete Members with Consideration of The Strain Rate Effect, Journal of Structural and Construction Engineering, No.482, pp. 83-92, Apr., 1996
4. Japanese Industrial Standards Committee, Japanese Industrial Standards B 0205, 1997